

SHIELD8-UAV: Sequential 8-bit Hardware Implementation of a Precision-Aware 1D-F-CNN for Low-Energy UAV Acoustic Detection and Temporal Tracking

Susmita Ghanta

Dept. of Electrical Engineering
Indian Institute of Technology Jammu
Jagti 181221, India
2024pvl0105@iitjammu.ac.in

Karan Nathwani

Dept. of Electrical Engineering
Indian Institute of Technology Jammu
Jagti 181221, India
karan.nathwani@iitjammu.ac.in

Rohit Chaurasiya

Dept. of Electrical Engineering
Indian Institute of Technology Jammu
Jagti 181221, India
rohit.chaurasiya@iitjammu.ac.in

Abstract—Real-time unmanned aerial vehicle (UAV) acoustic detection at the edge demands low-latency inference under strict power and hardware limits. This paper presents SHIELD8-UAV, a sequential 8-bit hardware implementation of a precision-aware 1D feature-driven CNN (1D-F-CNN) accelerator for continuous acoustic monitoring. The design performs layer-wise execution on a shared multi-precision datapath, eliminating the need for replicated processing elements. A layer-sensitivity quantisation framework supports FP32, BF16, INT8, and FXP8 modes, while structured channel pruning reduces the flattened feature dimension from 35,072 to 8,704 (75%), thereby lowering serialised dense-layer cycles. The model achieves 89.91% detection accuracy in FP32 with less than 2.5% degradation in 8-bit modes.

The accelerator uses 2,268 LUTs and 0.94 W power with 116 ms end-to-end latency, achieving 37.8% and 49.6% latency reduction compared with QuantMAC [1] and LPRE [2], respectively, on a Pynq-Z2 FPGA, and 5–9% lower logic usage than parallel designs. ASIC synthesis in UMC 40 nm technology shows a maximum operating frequency of 1.56 GHz, 3.29 mm² core area, and 1.65 W total power. These results demonstrate that sequential execution combined with precision-aware quantisation and serialisation-aware pruning enables practical low-energy edge inference without relying on massive parallelism.

Index Terms—UAV acoustic detection, 1D CNN, edge AI accelerator, sequential execution, precision-aware quantization, pruning, FPGA, ASIC

I. INTRODUCTION

The rapid growth of edge artificial intelligence (AI) has intensified the demand for energy-efficient neural network accelerators capable of real-time inference under constrained power and hardware budgets. Among emerging edge workloads, unmanned aerial vehicle (UAV) acoustic detection has gained significant attention for surveillance, security, and autonomous monitoring applications, where reliable operation is required under low-visibility and non-line-of-sight conditions. Conventional CNN accelerators primarily rely on spatial parallelism through replicated processing elements to achieve high throughput. While effective in data-centre environments, such architectures incur substantial area, memory bandwidth, and power overhead, making them unsuitable for edge deployments. Moreover, dense layers and high-precision computation further increase latency and energy consumption, limiting scalability on resource-constrained platforms.

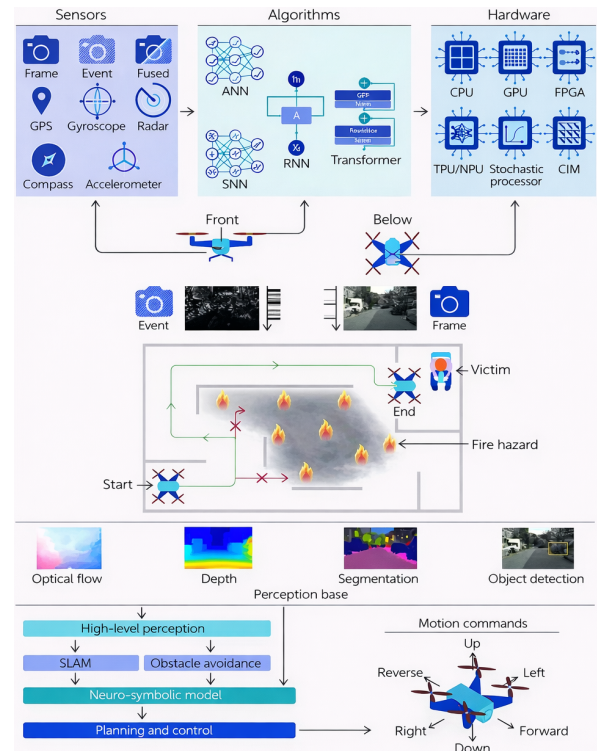


Fig. 1: Overview of the algorithm-hardware co-design stack for UAV acoustic detection and temporal tracking on edge platforms.

Recent research has explored model compression and low-precision inference to improve hardware efficiency; however, many existing designs still depend on partially parallel compute fabrics and lack unified hardware–algorithm co-optimisation. In particular, redundant datapath duplication and unstructured computation patterns lead to inefficient utilization of on-chip resources during sequential layer execution. Fig. 1 illustrates the proposed co-design stack spanning sensing, feature extraction, learning, and hardware mapping. Acoustic signals are converted into compact feature vectors, processed by the lightweight 1D-F-CNN, and executed on a sequential multi-precision accelerator with shared datapath reuse. The

layer-wise precision-aware quantisation, (iii) structured pruning for serialisation-aware optimisation, and (iv) a reusable multi-precision sequential accelerator architecture.

A. Feature-Driven 1D-F-CNN for UAV Detection

The proposed model operates on compact acoustic feature vectors extracted from short-duration audio segments, avoiding computationally expensive 2D spectrogram processing. This design reduces memory footprint, feature-map storage, and data movement, enabling efficient hardware mapping.

Given an input feature vector $\mathbf{x} \in \mathbb{R}^{1 \times M}$, each convolutional block performs 1D convolution followed by activation, pooling, and regularisation:

$$\mathbf{o} = \mathcal{D}_{0.2} \left(\mathcal{M}_{1 \times 2} \left(\sigma_R \left(\mathcal{C}_{1 \times 3}(\mathbf{x}) \right) \right) \right), \quad (1)$$

where $\mathcal{C}_{1 \times 3}$ denotes the 1D convolution, $\sigma_R(\cdot)$ is ReLU, $\mathcal{M}_{1 \times 2}$ represents max-pooling, and $\mathcal{D}_{0.2}$ denotes dropout. Three convolutional stages capture temporal acoustic patterns such as rotor harmonics and periodic signatures, followed by dense layers for binary classification. Compared to 2D CNNs, the 1D architecture significantly reduces parameter count and intermediate feature size while preserving discriminative temporal representation [3].

B. Precision-Aware Quantisation With Layer Sensitivity

To balance accuracy and hardware efficiency, a layer-wise precision assignment strategy is employed based on quantisation sensitivity. For each layer l , a sensitivity score is defined as

$$s_{l,sc,k} = \frac{\left(\left\| Q^{\text{PwQ}}(\mathbf{w}_l) - \mathbf{w}_l \right\| - \left\| Q_{sc,k}^{\text{PwQ}}(\mathbf{w}_l) - \mathbf{w}_l \right\| \right) \cdot \|\nabla \mathcal{L}_{\mathbf{w}_l}\|}{n_l} \quad (2)$$

$$s_l = \max(s_{l,sc,16}, s_{l,sc,8}), \quad (3)$$

where \mathbf{w}_l and n_l denote the weights and size of layer l , respectively. Layers with higher sensitivity are assigned higher precision (FP32/BF16), while less sensitive layers operate in INT8 or FXP8 to reduce arithmetic cost.

Weights are quantised using learned clipping bounds W_l and W_h . For a full-precision weight W and bit-width n , the scale factor is

$$\text{scale}(k) = \text{mean}(|W|) \cdot \frac{2^n - 1}{2^{n-1}}, \quad (4)$$

and the integer quantised weight is

$$\widehat{W} = \text{round} \left(\left(\text{clip} \left(\frac{W}{k}, W_l, W_h \right) - W_l \right) \cdot \frac{2^n - 1}{W_h - W_l} \right), \quad (5)$$

with reconstruction

$$Q^{\text{PwQ}}(W) = \widehat{W} \cdot \frac{W_h - W_l}{2^n - 1} + W_l. \quad (6)$$

Activation quantisation follows the PACT formulation with a learnable clipping parameter α :

$$y = \text{PACT}(x) = 0.5 (|x| - |x - \alpha| + \alpha), \quad (7)$$

TABLE I: Dense-Layer Feature Reduction and Hardware Benefits

Metric	Before Pruning [3]	After Pruning
Flatten size	35,072	8,704
Size reduction	75%	
Dense MACs	Very high	$\approx 75\%$ lower
Serialized cycles	35,072	8,704
Design debug	High	Reduced
Timing & power	Challenging	Improved

$$x^q = \text{round} \left(y \cdot \frac{2^n - 1}{\alpha} \right) \cdot \frac{\alpha}{2^n - 1}. \quad (8)$$

This formulation enables flexible multi-precision inference across FP32, BF16, INT8, and FXP8 modes while preserving detection accuracy compared to [1].

C. Structured Pruning for Serialisation-Aware Optimisation

In sequential accelerators, the flatten-to-dense interface becomes a dominant latency bottleneck due to serialised data movement through a shared datapath. To address this, structured channel pruning is applied before flattening, reducing the feature dimension from 35,072 to 8,704. This directly decreases dense-layer MAC operations and execution cycles in serialized hardware pipelines. Unlike conventional compression-oriented pruning, the objective here is scheduling-aware optimisation that improves latency, simulation efficiency, and verification feasibility in reusable accelerator designs. Table I discusses the implications in detail.

D. Sequential Multi-Precision Accelerator Architecture

The proposed POLARON accelerator adopts a reusable shared-compute datapath composed of input and weight buffers, a configurable MAC bank, accumulation and activation units, and an FSM-based control engine (Fig. 3). All neural network layers execute sequentially on the same compute fabric, avoiding dedicated per-layer processing elements and thereby reducing area and control complexity. Feature maps and weights are streamed from on-chip buffers to the MAC bank, and intermediate activations are written back to local memory for reuse in subsequent layers. The datapath supports FP32, BF16, INT8, and FXP8 computations via programmable alignment and scaling logic, while extended-precision accumulators maintain numerical stability during reduced-precision operations. The controller orchestrates convolution, pooling, and fully connected operations within a unified execution pipeline for end-to-end network inference.

Communication with the host system is via an AXI interface, with AXI-Lite for configuration and AXI-DMA/Stream for data transfer. Incoming data is staged in on-chip feature memory prior to computation. Per-layer precision selection allows adaptation of numeric format based on workload requirements to balance energy and accuracy. After accumulation, results pass through normalization, scale-and-shift, and overflow handling before entering a CORDIC-based activation unit supporting Swish, SoftMax, SeLU, GELU, Sigmoid, Tanh, and ReLU. A configuration prefetcher interprets layer

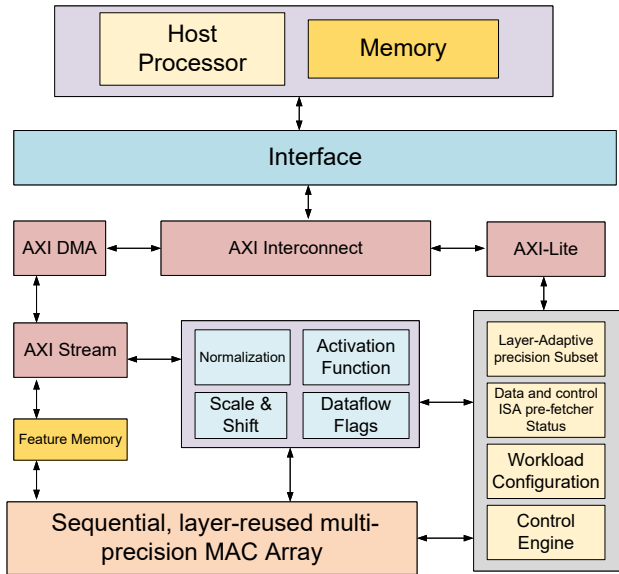


Fig. 3: Proposed precision-aware sequential accelerator architecture with shared compute and multi-precision support.

metadata and updates execution parameters at runtime. The resulting dataflow minimizes memory traffic and latency while enabling precision-aware inference for edge-AI workloads.

IV. METHODOLOGY AND EXPERIMENTAL SETUP

A. Dataset Preparation and Augmentation

A heterogeneous acoustic dataset comprising UAV and non-UAV environmental sounds was curated to emulate realistic deployment conditions. UAV recordings were collected from multiple commercial quadrotor platforms at different distances and orientations to capture rotor harmonics, startup transients, and flight-state variations. Background samples include environmental and aircraft-related audio representative of open-field and airport scenarios.

To improve robustness, recordings were augmented with additive Gaussian noise across a controlled SNR range. Each audio stream was segmented into 0.8-second windows to balance temporal feature capture and inference latency, followed by amplitude normalisation to ensure consistent scaling across samples. Feature extraction was performed using *librosa*, including MFCC, pooled mel-spectrogram coefficients, power spectral density (PSD), and zero-crossing rate (ZCR), enabling representation of both periodic rotor signatures and broadband acoustic activity. Public audio repositories (e.g., AudioSet and Pixabay) were additionally incorporated to enhance background diversity and reduce environment-specific bias [3].

B. Training and Evaluation Metrics

The dataset was partitioned into training, validation, and test sets for unbiased evaluation. Model training employed the Adam optimiser with cross-entropy loss and early stopping based on validation performance. Detection performance is reported using accuracy, precision, recall, and F1-score. Given

TABLE II: Evaluation Metrics for UAV Detection Models

Model	Features	Acc. (%)	Prec. (%)	Rec. (%)	F1 (%)
SVM [8]	Mel (128)	87.88	88.41	87.44	87.92
	MFCC (20)	84.39	85.62	83.17	84.37
	$\log_{10}(\text{PSD})$	83.10	80.23	88.43	84.13
1D-R-CNN [3]	Raw audio	88.90	92.78	84.54	88.47
2D-CNN [9]	MFCC (20)	88.96	88.85	89.32	89.09
KNN [8]	MFCC (20)	88.73	87.87	90.21	89.02
Ensemble [10]	Mel (128)	86.50	86.88	85.55	86.21
1D-M-CNN [11]	MFCC (128)	83.26	86.11	85.52	85.81
Baseline (FP32)	Mel (128)	89.13	91.64	86.48	88.99
	MFCC (20)	89.91	89.00	91.39	90.18
	$\log_{10}(\text{PSD})$	87.87	88.88	86.92	87.89
	ZCR	60.64	58.61	77.58	66.77
Proposed (BF16)	Mel (128)	88.94	91.42	86.21	88.71
	MFCC (20)	89.80	88.89	91.28	90.07
	$\log_{10}(\text{PSD})$	87.65	88.65	86.68	87.66
	ZCR	60.14	58.11	77.08	66.27
Proposed (INT8)	Mel (128)	88.02	90.31	85.06	87.73
	MFCC (20)	89.14	88.23	90.62	89.41
	$\log_{10}(\text{PSD})$	86.55	87.56	85.60	86.57
	ZCR	57.34	55.31	74.28	63.47
Proposed (FXP8)	Mel (128)	87.65	89.88	84.72	87.02
	MFCC (20)	88.97	88.06	90.45	89.24
	$\log_{10}(\text{PSD})$	86.02	87.03	85.07	86.04
	ZCR	55.40	53.37	72.34	61.53

the requirements of continuous monitoring systems, false alarm rate and missed detection rate are also evaluated to assess practical reliability. Robustness was further analysed by measuring inference accuracy across varying SNR levels, reflecting realistic noisy deployment scenarios.

C. Algorithm-Hardware Co-Design Evaluation

The proposed framework was validated through both algorithm-level emulation and hardware implementation. A Python-based arithmetic emulation model was developed to analyse inference behavior under FP32, BF16, INT8, and FXP8 precision formats prior to RTL realisation. The accelerator was implemented in Verilog HDL and verified using cycle-accurate simulation. FPGA synthesis was performed using the AMD Vivado toolchain on the Pynq-Z2 platform, while ASIC synthesis was conducted using Cadence Genus targeting a UMC 40 nm CMOS technology library under uniform timing constraints. For fair comparison, representative baseline accelerators were evaluated under normalised assumptions where required. Hardware metrics include LUT/DSP utilisation, operating frequency, power, and estimated area, while system-level evaluation considers end-to-end inference latency and energy consumption during continuous operation.

V. RESULTS AND DISCUSSION

A. Detection Performance and Precision Impact

Table II summarises the detection performance of the proposed 1D-F-CNN against classical and deep-learning baselines. Using MFCC features in FP32 mode, the model achieves 89.91% accuracy and 90.18% F1-score, demonstrating competitive performance while operating on a compact feature representation. BF16 inference exhibits near-identical accuracy to FP32, indicating low sensitivity to mantissa reduction. INT8 and FXP8 show moderate degradation but remain suitable for

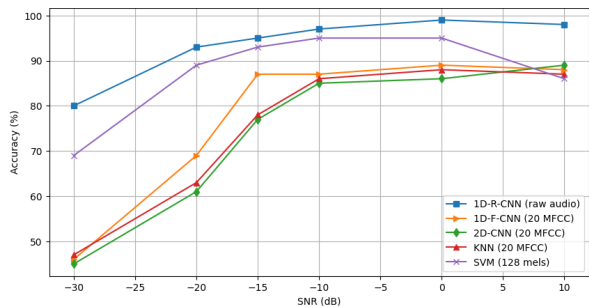


Fig. 4: Detection accuracy versus signal-to-noise ratio (SNR).

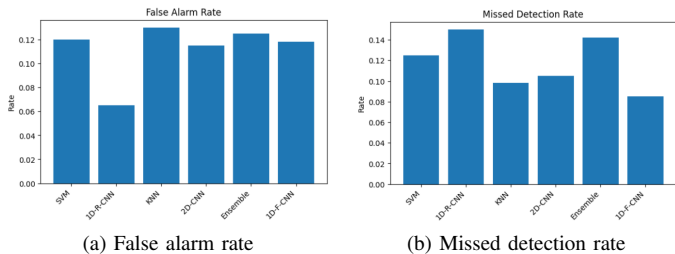


Fig. 5: Error analysis under noise conditions: (a) false alarm rate and (b) missed detection rate. False alarms remain at low SNR levels, while missed detections increase when UAV acoustic signatures are impacted by background noise.

practical monitoring scenarios. These results validate the layer-wise precision-aware quantisation strategy in maintaining accuracy under reduced numerical precision.

Fig. 4 presents accuracy trends across varying SNR levels, and Fig. 5 shows false alarm and missed detection behavior. The model maintains stable performance under moderate noise, reflecting effective capture of rotor acoustic patterns. False alarms remain low across most SNR ranges, while missed detections increase only at very low SNR due to masking of harmonic signatures. Overall, the feature-driven 1D architecture demonstrates robustness for continuous real-world monitoring. Table I shows structured pruning reduces the flattened feature size from 35,072 to 8,704 (75%), thereby proportionally lowering the number of dense-layer cycles in the sequential shared datapath. Thus, pruning improves not only model compactness but also inference latency and hardware verification efficiency.

B. Hardware Utilization

Table III compares the proposed architecture with representative FPGA accelerator styles. Fully parallel designs achieve high throughput at the cost of significant LUT, register, and DSP usage. In contrast, the proposed sequential architecture employs a unified compute datapath, minimising resource duplication while preserving functional flexibility. As a result, the design achieves lower hardware utilisation than parallel or partially reusable accelerators. Table IV further confirms that competitive performance and lower resource overhead through compute reuse and precision adaptation.

TABLE III: FPGA resource utilisation comparison with representative architectural baselines

Architecture	LUTs	Reg./FFs	BRAM/DSPs	Power (W)
Fully-parallel [13]	20790	30684	53	2.2
Hardware-reused [1]	14428	15582	23	1.28
Layer-reused [14]	13956	16323	24	1.24
Layer-multiplexed [15]	11265	11348	32	0.73
Proposed (SHIELD8-UAV)	2,268	3250	8	0.94

TABLE IV: Quantitative FPGA comparison with prior architectural works

Parameters	Lu et al. [16]	Aimar et al. [17]	Mian et al. [18]	RAMAN [19]	Proposed
Platform	Zynq-7100	VC707	ZCU102	Efinix Ti60	VC707
Model	CNN	CNN	1D-CNN	DS-CNN	1D-F-CNN
LUTs (K)	22.9	23.9	39	37.2	2.2
Reg./FFs (K)	10.7	20.1	27.8	8.6	3.25
Power (W)	1.1	2.2	1.54	0.15	0.94
Freq. (MHz)	60	170	200	75	100

ASIC synthesis results at 40 nm (Table V) indicate a balanced trade-off between frequency, area, and power. Unlike massively parallel accelerators that prioritise peak throughput, the proposed design targets sustained inference efficiency suitable for continuous sensing workloads. The shared multi-precision datapath reduces switching activity and enables scalable deployment across different energy budgets.

C. System-Level Latency and Energy

A cycle-accurate timing model was developed to analyse latency for reusable and parallel accelerator architectures, as defined in Eqs. 9 and 10. The complete system was deployed on the Pynq-Z2 platform for end-to-end evaluation. The proposed accelerator achieves 116 ms inference latency under constrained power ($\leq 5W$), outperforming prior reusable and edge platforms, including Flex-PE [12] (186.4 ms), GR-ACMTr [13] (772 ms), LPRE [2] (184 ms), QuantMAC [1] (163.7 ms), Jetson Nano (226 ms), and Raspberry Pi (555 ms).

$$T_P = T_{MAC} + T_{AF},$$

$$T_R = T_{MAC} + T_{Serial} + K \cdot T_{AF},$$

where T_{MAC} , T_{AF} , T_{PISO} is delay for MAC, and serial AF. (9)

$$Total_T_P = \sum_{l=1}^{L-1} n(l) + L - 1,$$

$$Total_T_R = \sum_{l=1}^L n(l) + 2L - 3,$$

where L and $n(l)$: no. of layers and MACs in layer.

Compared to prior reusable accelerators, the proposed system achieves lower latency and competitive energy efficiency. The improvement is primarily attributed to reduced dense-layer serialisation, precision-aware arithmetic, and unified compute reuse, which collectively minimise memory transfers and execution overhead. Fig. 6 summarises the overall system

TABLE V: Post-synthesis ASIC evaluation metrics at 40 nm for diverse AI accelerators

Design	Freq. (GHz)	Area (mm ²)	Power (W)
JSSC'25 [20]	1.25	2.12	1.22
TVLSI'25 [21]	2.05	3.67	1.08
TVLSI'25 [12]	0.53	4.85	0.47
ISCAS'25 [14]	1.93	4.73	5.71
TCAS-I'22 [22]	1.46	10.80	1.02
TRETS'23 [13]	1.18	4.77	1.82
Proposed	1.56	3.29	1.65

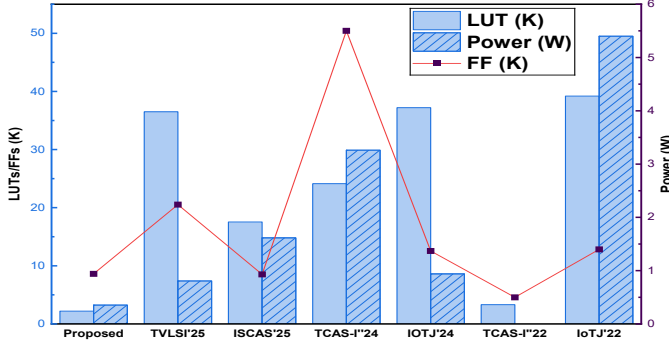


Fig. 6: System-level performance summary.

performance, demonstrating that sequential execution combined with hardware-aware co-design enables practical real-time edge inference.

VI. CONCLUSION & FUTURE WORK

This paper presented SHIELD8-UAV, a precision-aware sequential 1D-F-CNN accelerator for continuous UAV acoustic monitoring on resource-constrained edge platforms. By combining reusable layer-wise execution, multi-precision computation, and serialisation-aware optimisation, the proposed system achieves 89.91% detection accuracy with less than 2.5% degradation under 8-bit inference (INT8/FXP8). Structured channel pruning reduces the flattened feature dimension from 35,072 to 8,704 (75% reduction), directly lowering dense-layer serialisation cycles and verification overhead.

Hardware results validate practical edge deployment: the FPGA implementation consumes 2,268 LUTs and 0.94 W while achieving 116 ms end-to-end latency, outperforming prior accelerators (QuantMAC, LPRE) and embedded platforms (Jetson Nano, Raspberry Pi). ASIC synthesis at 40nm reaches 1.56 GHz within a 3.29mm² area and 1.65W power, confirming scalability beyond FPGA prototyping. Future work will explore runtime adaptive precision control and extension to multi-class acoustic scene recognition.

REFERENCES

- [1] N. Ashar, G. Raut, *et al.*, “QuantMAC: Enhancing Hardware Performance in DNNs With Quantize Enabled Multiply-Accumulate Unit,” *IEEE Access*, vol. 12, pp. 43600–43614, 2024.
- [2] O. Kokane, M. Lokhande, G. Raut, A. Teman, and S. K. Vishvakarma, “LPRE: Logarithmic Posit-enabled Reconfigurable edge-AI Engine,” in *IEEE International Symposium on Circuits and Systems*, pp. 1–5, 2025.
- [3] M. Ali and K. Nathwani, “Exploiting wavelet scattering transform and 1d-cnn for unmanned aerial vehicle detection,” *IEEE Signal Processing Letters*, vol. 31, pp. 1790–1794, 2024.
- [4] Y. Wang, Z. Chu, I. Ku, E. C. Smith, and E. T. Matson, “A large-scale uav audio dataset and audio-based uav classification using cnn,” in *IEEE International Conference on Robot and Computing*, pp. 186–189, 2022.
- [5] S. Abdoli, P. Cardinal, and A. L. Koerich, “End-to-end environmental sound classification using a 1d convolutional neural network,” *Expert Systems with Applications*, vol. 136, pp. 252–263, 2019.
- [6] M. Lokhande, A. Jain, and S. K. Vishvakarma, “Precision-aware On-device Learning and Adaptive Runtime-cONfigurable AI acceleration,” *IEEE International Symposium on VLSI Design and Test*, Aug. 2025.
- [7] T. Norrie, N. Patil, and D. H. Yoon, “The design process for google tpuv2 and tpuv3,” *IEEE Micro*, vol. 41, pp. 56–63, 2022.
- [8] M. Anwar, Z. Kaleem, and A. Jamalipour, “ML-inspired sound-based amateur drone detection for public safety applications,” in *IEEE Transactions on Vehicular Technology*, vol. 68, pp. 2526–2534, 2019.
- [9] G. Raj, R. I. S. Mathew, and L. R. Cenkeramaddi, “Aerial vehicle classification using a custom lightweight cnn: A deep learning approach,” in *2025 IEEE International Conference on Electronics, Computing and Communication Technologies (CONECT)*, pp. 1–6, 2025.
- [10] J. McCoy, A. Rawal, D. B. Rawat, and B. M. Sadler, “Ensemble dl for sustainable multimodal uav classification,” *IEEE Trans. on Intelligent Transportation Syst.*, vol. 24, no. 12, pp. 15425–15434, 2023.
- [11] V. K. Puduru, B. Pardhasaradhi, S. Koorapati, and L. R. Cenkeramaddi, “Lightweight deep learning model for airborne object classification,” in *2025 IEEE 14th International Conference on Communication Systems and Network Technologies (CSNT)*, pp. 230–234, 2025.
- [12] M. Lokhande, G. Raut, and S. K. Vishvakarma, “Flex-PE: Flexible and SIMD Multiprecision Processing Element for AI Workloads,” *IEEE Trans. VLSI Syst.*, vol. 33, no. 6, pp. 1610–1623, 2025.
- [13] G. Raut, S. Karkun, and S. K. Vishvakarma, “An Empirical Approach to Enhance Performance for Scalable CORDIC-Based DNNs,” *ACM Trans. Reconfigurable Technol. Syst.*, vol. 16, June 2023.
- [14] O. Kokane, G. Raut, S. Ullah, *et al.*, “Retrospective: A CORDIC-Based Configurable Activation Function for NN Applications,” *IEEE Computer Society Annual Symposium on VLSI (ISVLSI)*, 2025.
- [15] G. Raut, A. Biasizzo, N. Dhakad, N. Gupta, G. Papa, and S. K. Vishvakarma, “Data multiplexed and hardware reused architecture for DNN accelerator,” *Neurocomputing*, vol. 486, pp. 147–159, 2022.
- [16] J. Lu, D. Liu, X. Cheng, *et al.*, “An efficient unstructured sparse cnn accelerator for wearable ecg classification device,” *IEEE Trans. on Circ. and Syst. I*, vol. 69, no. 11, pp. 4572–4582, 2022.
- [17] A. Aimar, H. Mostafa, *et al.*, “Nullhop: A flexible cnn accelerator based on sparse representations of feature maps,” *IEEE Trans. on NN and Learning Systems*, vol. 30, no. 3, pp. 644–656, 2019.
- [18] F. A. Mian and S. Zafar, “SoC-Based Implementation of 1-D CNN for 3-Channel ECG Arrhythmia Classification via HLS4ML,” *IEEE Embedded Systems Letters*, vol. 16, no. 4, pp. 429–432, 2024.
- [19] A. Krishna, S. Rohit Nudurupati, *et al.*, “RAMAN: A Reconfigurable and Sparse tinyML Accelerator for Inference on Edge,” *IEEE Internet of Things Journal*, vol. 11, no. 14, pp. 24831–24845, 2024.
- [20] K. Li, M. Huang, A. Li, *et al.*, “A 29.12-tops/w vector systolic accelerator with nas-optimized dnn in 28-nm cmos,” *IEEE Journal of Solid-State Circuits*, vol. 60, no. 10, pp. 3790–3801, 2025.
- [21] S. M. Cherati, M. Barzegar, and L. Sousa, “MSDF-Based MAC for Energy-Efficient Neural Networks,” *IEEE Trans. on Very Large Scale Integr. Syst.*, pp. 1–12, Feb. 2025.
- [22] R. Pilipović, P. Bulić, and U. Lotrič, “A Two-Stage Operand Trimming Approximate Logarithmic Multiplier,” *IEEE Transactions on Circuits and Systems I: Regular Papers*, vol. 68, pp. 2535–2545, June 2021.